Ocean Engineering 184 (2019) 1–10

Contents lists available at ScienceDirect

Ocean Engineering

journal homepage: www.elsevier.com/locate/oceaneng

A multilayer path planner for a USV under complex marine environments

Ning Wang [a,*], Xiaozhao Jin [a], Meng Joo Er [b]

[a] Center for Intelligent Marine Vehicles, School of Marine Electrical Engineering, Dalian Maritime University, Dalian, 116026, PR China
[b] School of Electrical and Electronic Engineering, Nanyang Technological University, 639798, Singapore

ARTICLE INFO

Keywords:
Multilayer path planner
Collision avoidance
Routine correction
Stochastic dynamic coastal environment
Fast marching method

ABSTRACT

In this paper, a multilayer path planner (MPP) with global path-planning (GPP), collision avoidance (CA) and routine correction (RC) for an unmanned surface vehicle (USV) under complex marine environments including both coastal and surface constraints is presented. The main contributions of this paper are as follow: 1) An MPP framework consisting of multiple layers, i.e., backbone, CA and RC, is established, and achieves self-tuning path-planning which adapts time-varying environments. 2) To minimize yaw-cost for the USV within local path, a novel CA algorithm is developed by the B-Spline method. 3) For capturing environmental influences arisen from reefs around the coastline, a stochastic dynamic coastal environments (SDCE) model is built by virtue of Poisson distribution. In combination with the fast marching method (FMM) and the SCDE model, the RC algorithm is proposed to handle environmental uncertainties. Simulation results show that the proposed MPP achieves remarkable path-planning performance in terms of both collision avoidance and adaptability to complex environments.

1. Introduction

Currently, with the increasing usage of unmanned surface vehicle (USV), many studies have spread around promising technologies (Wang et al., 2017; Wang et al., 2019a; Wang et al., 2019b; Wang et al., 2018a; Wang et al., 2018b; Qin, Wu, Sun, Chen). Meanwhile, a path planning technique with high safety and efficiency plays an essential role in applying the USV to real-world maritime environments. To be specific, the USV needs path planning methods to autonomously perform various tasks including coastal patrols and rescues, *etc*. To this end, in addition global approaches, tools for local collision avoidance (CA) and route correction (RC) become critical within the whole path planning scheme. As a consequence, both global and local path planning strategies are highly desired to be utilized, simultaneously.

In the earlier stage, path planners mainly focused on GPP approaches, whereby heuristic algorithms were popularly employed. In (Hart et al., 1972), a formal mathematical framework including A* method has been established to minimize path costs. It should be noted that the traditional A* approach is exclusively designed for static environments. As a result, if the environment happens to change rapidly and/or suddenly, the global-sense path planning approaches like A* would become unavailable since re-optimization burden definitely requires unexpectedly overlong computation time. In this context, to solve the foregoing problem, various improvements on A* method were conducted in the literature. In (Stentz, 1995; Ferguson and Stentz, 2006), a dynamic A* algorithm with its extensions have been proposed to reduce total planning time by re-planning accurate path at arbitrary position. By using a modified A* method in (Ammar et al., 2016; Phanthong et al., 2014), GPP problem of a robot was solved by establishing an approximation to the optimal path. In terms of decreasing computation time, the modified A* algorithm constructed another version without visiting any cell more than once. However, the vehicle cannot consider real-world environments which may include unknown static/dynamic obstacles. In (Phanthong et al., 2014), an A*-based algorithm has been used to compute near-optimal paths considering underwater obstacles in ocean environments. However, the heuristic methods were mainly responsible for planning path in global or static environments, excluding local planning. If there is no crashworthiness (Pawlus et al., 2013), the vehicle is likely to be damaged. Hence, global approaches, like A* and its variants, are unsuitable for CA and RC.

In the literature, a series of dynamic local path planning algorithms, including genetic algorithm (Kim et al., 2017; Kanakakis and Tsourveloudis, 2007; Leigh et al., 2007; Tanakikorn et al., 2014), ant colony optimization (Vinay and Sridharan, 2012; Chen et al., 2013; Wu et al., 2016a) and particle swarm optimization (Roberge et al., 2013; Li et al., 2006), have been proposed. It should be noted that foregoing

* Corresponding author.
E-mail addresses: n.wang.dmu.cn@gmail.com (N. Wang), j1009935031@sina.cn (X. Jin), emjer@ntu.edu.sg (M.J. Er).

https://doi.org/10.1016/j.oceaneng.2019.05.017
Received 29 November 2018; Received in revised form 7 May 2019; Accepted 8 May 2019

evolutionary algorithms did not consider suboptimal problems, and thereby resulting that the optimization of path length, and the convergence and consistency cannot be guaranteed. Alternatively, the artificial potential field (APF) method (Khatib, 1986) can characterize the influence of obstacles and target points in real-time by generating a potential field including the repulsive and attractive forces. Hence, successive path points can be rapidly determined by the APF algorithm which might be regarded as a potential tool to solve local optimization of path planning for a USV. Variants of the APF in (Wu et al., 2016b; Pan et al., 2014; Li et al., 2016; Kim et al., 2016; Min et al., 2015; Sethian., 1996; Garrido et al., 2006; Wang et al., 2018c, 2018d; Zhou et al., 2018; Liu and Bucknall, 2015, 2017; Song et al., 2017; Richards and How, 2002; Liu et al., 2017) have also been proposed to address dynamic obstacles avoidance. However, the vital drawback, i.e., local minimum, pertaining to the APF inevitably renders the vehicle stagnant or trapped.

Recently, the fast marching method (FMM) (Sethian., 1996) was proposed to artificially simulate the propagation process of an electromagnetic wave that starts from the original point. Basically, the farther away from the original point, the higher the potential value. In this context, the original point of propagation can be set as the goal point such that there exists only one minimum locating at the goal. In (Garrido et al., 2006), the FMM has been used to obtain the path with characteristics of speed and reliability. In (Wang et al., 2018c), an FMM-based path-planning scheme between two points has been developed with an additional minimization step. A multi-player differential problem called reach-avoid game in (Zhou et al., 2018) has been solved by deploying the FMM. In (Liu and Bucknall, 2017), a safety parameter has been introduced into the FMM so that CA capability can be ensured in a constrained environment. In (Song et al., 2017; Liu and Bucknall, 2015), path planning for a USV in practical environments has also been proposed by modifying the FMM. However, the generated paths can only guarantee sub-optimal solutions.

Furthermore, considering vehicle dynamics and/or constraints, a trajectory, rather than a path, is highly required to be planned. In the literature, dynamic constraints in known environments have been addressed. In (Richards and How, 2002), a cooperative planning scheme for multiple aircrafts with CA has been developed. A trajectory planning method for parking has been devised in (Liu et al., 2017), whereby vehicle dynamic constraints can be matched. It should be noted that these aforementioned algorithms neglected stochastic uncertainties and dynamic constrains in complex environments. Actually, complex uncertainties and/or unknown dynamics (Wang et al., 2018d, 2018e) are highly desired to be addressed in practice. In (Park et al., 2018), the stochastic environmental dynamics were modeled by Gaussian distributions. In (Shin and Mckay, 1986), a solution to minimizing the cost along a geometric path has been provided by using the dynamic programming. For autonomous underwater vehicle path-planning, a planning algorithm, which includes terrain dynamic matching algorithm, search length, min-length, cost function, dynamic path-planning and second-goal point algorithm, was proposed based on A* algorithm in (Li. et al., 2017a). In (Li. et al., 2017b), an improved terrain correlation correction method is proposed to correct the inertial navigation system error of the prior marine map. However, foregoing algorithms cannot capture complex marine environments including reefs and dynamic obstacles. In this context, a promising path-planning scheme which can address complex environments covering both surface and reefs is highly desirable. To be specific, both RC and CA under complex marine environments with coastal and/or dynamic obstacles should be handled, simultaneously.

In this paper, we focus on an unresolved problem that, in the presence of static obstacles, dynamic obstacles, and reefs, the CA and RC are addressed based on the GPP with FMM. By defining a series of functions, the entire MPP is formulated in a path-planning scheme consisting of backbone layer, CA layer and RC layer in the complex environments including both coastal and surface constraints. In order to avoid dynamic obstacle, an auxiliary system for optimizing original CA path is designed to minimize its yaw-cost. The coastal environments is built to exactly estimate influence range of reefs by Poisson distribution. In combination with GPP by FMM, the novel multilayer path planner (MPP) are eventually presented. Unlike previous approaches, the proposed path-planning scheme not only estimates special environments, but also generates suitable path for a USV.

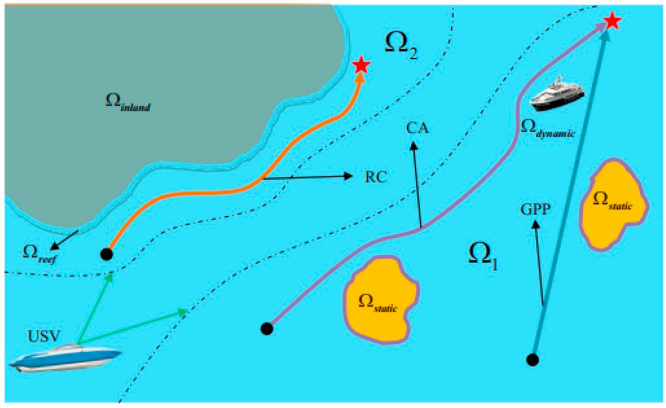

Fig. 1. Illustration of the complex marine environments.

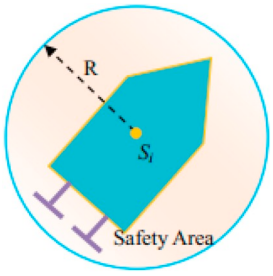

Fig. 2. Safety area of the USV.

The rest of this paper is organized as follow. In Section 2, preliminaries and problem formulation are briefly described. In Section 3, the proposed multilayer path-planning scheme of USV path planner is developed by addressing not only GPP, but also CA and RC in the complex marine environments. Simulation results in the complex environments are presented in Section 4. The conclusions are presented in Section 5.

2. Problem Formulation

This paper describes the complex marine environments Ω_X including both marine surface domain Ω_1 and coastal domain Ω_2, where $X = (x, y)$ represents the position in Ω_X. The illustration of the complex marine environments is shown in Fig. 1, the marine surface domain Ω_1 has two kinds of obstacles:

$$\Omega_1 = \Omega_{movable} \cup \Omega_{static} \cup \Omega_{dynamic}(T_d) \tag{1}$$

where $\Omega_{movable}$ is the movable space for the USV, Ω_{static} represents the domain of the static obstacles that need to be globally path planned on $\Omega_{movable}$, $\Omega_{dynamic}$ corresponds to dynamic obstacles which are the objects of collision avoidance (CA), while the T_d is the moment when dynamic obstacle appear.

In addition, as shown in Fig. 2, an orange area of the USV with safety radius R is expected to be strictly inviolable during path-planning, To be specific, this safety area with R is determined by:

$$C_R(t) = \left\{ |S_i| \middle\| S_i - \Omega_{dynamic}(T_d) \right\| \geq R \} \tag{2}$$

where $S_i = [S_{i(x)}, S_{i(y)}]^T$ represents the position of the USV at the ith

moment. When the dynamic obstacle enters this area, the USV begins to avoid collision. Meanwhile, the energy consumption E_{CA} of *CA* action is derived from the yaw ψ_i changing. In order to save the energy of the USV, E_{CA} should have a maximum limit, as follows:

$$C_{\varphi} = \left\{ E_{CA} \middle| \sum E_{CA} \leq E_{max} \right\} \tag{3}$$

where E_{max} is the maximum energy consumption of the *CA* path.

The coastal domain Ω_2 can be partitioned as:

$$\Omega_2 = \Omega_{inland} \cup \Omega_{reef}(t) \tag{4}$$

where Ω_{inland} is a compact set representing the inland space in which the USV can not move, while $\Omega_{reef}(t)$ corresponds to reefs whose uncertain influence ranges Θ are randomly varied by water levels w changing. To be specific, the coastal constraints is determined by:

$$C_r(t) = \left\{ \Omega_{reef}(t) \middle| \Theta \in SCDE(w_t) \right\} \tag{5}$$

where $SCDE(\bullet)$ is the stochastic dynamic coastal environments (SCDE) model within the water level w_t, and the t is the moment when the USV detects the w and performs route correction (RC) in this domain.

In this context, given *a priori* knowledge on these constraints C_{um} which not allows a USV to move in domain Ω_{um} consisting of Ω_{inland} and Ω_{static}, together with movable conditions C_m on the sea surface:

$$C_{um} = \{ \Omega_{unmovable} | f(\Omega_{inland}, \Omega_{static}) = 0 \} \tag{6}$$

$$C_m = \{ \Omega_{movable} | f(\Omega_{movable}) = 1 \} \tag{7}$$

where $f(\bullet)$ is appropriate function reflecting the degree of mobility in these constraints and/or conditions. 0 and 1 represent completely unmovable and movable, respectively. The aim of this paper is to design the MPP for the USV in foregoing complex marine environments with these *C*, respectively, such that *GPP*, *CA* and *RC* in terms of length, safety and efficiency, *etc.*, have good results within the problem domains:

$$\begin{cases} C_{um} \cup C_m : GPP \\ C_{um} \cup C_m \cup C_R \cup C_{\varphi} : CA \\ C_{um} \cup C_m \cup C_r : RC \end{cases} \tag{8}$$

3. Multilayer path planning scheme

In this section, a multilayer path-planning scheme is created by both design marine environments and searching paths, simultaneously, and thereby facilitating the implementation of each layer's function solving the above problem domains.

3.1. Backbone layer

3.1.1. Global division

In order to divide the movable and unmovable domains, i.e., $\Omega_{unmovable}$ and $\Omega_{movable}$, within the whole map domain Ω_X, the gray-scale map $M_g(g_{(x,y)})$ is obtained by gray processing the original color map $M_o(R_{(x,y)}, G_{(x,y)}, B_{(x,y)})$ from the camera on the USV. To be specific, a gray-scale map $M_g(g_{(x,y)})$ can be characterized as follows:

$$g_{(x,y)} = \omega_1 R_{(x,y)} + \omega_2 G_{(x,y)} + \omega_3 B_{(x,y)} \tag{9}$$

where *R*, *G* and *B* are the degree of the red, green and blue, respectively, ω is the weight of these colors defined by the weighted average method to initialize the graysacle of the map.

In addition, there are two initialization cluster centers μ_1 and μ_2 of groups g_1 and g_2:

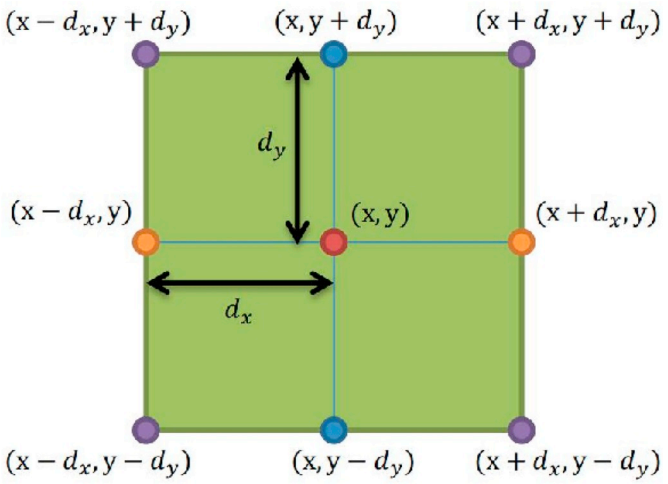

Fig. 3. Illustration of FMM.

$$g = \begin{cases} g_1 \supseteq \mu_1 \\ g_2 \supseteq \mu_2 \end{cases} \tag{10}$$

and the final cluster centers $\overline{\mu}$ are obtained by refining iteratively with K-Means clustering algorithm. The objective function is expressed as follows:

$$\{\overline{\mu}_1, \overline{\mu}_2\} = \arg\min_{\mu} \sum_{i}^{2} \sum_{g_{(x,y)} \in g_i} \left\| g_{(x,y)} - \mu_i \right\| \tag{11}$$

In order to clearly partition C_m and C_{um}, we set the gray value of C_m and C_{um} to 255 and 0, respectively:

$$\overline{g}_{(x,y)} = \begin{cases} 0, g_{(x,y)} < \delta \\ 255, g_{(x,y)} \geq \delta \end{cases} \tag{12}$$

where δ is a threshold that equal to $\frac{\overline{\mu}_1 + \overline{\mu}_2}{2}$.

Combined with Eqs. (6), (7) and (12), as follows:

$$\begin{cases} C_u m = \left\{ \Omega_{unmovable} | f = 0, \overline{g}_{(x,y)} = 0 \right\} \\ C_m = \left\{ \Omega_{movable} | f = 1, \overline{g}_{(x,y)} = 255 \right\} \end{cases} \tag{13}$$

3.1.2. Global Path Planning

In this section, the traditional FMM is the main method used to generate global path under the static constraints $C_{m \cup um}$. The FMM is a level-set method that was first proposed by Sethian to solve the Eikonal equation, which simulates the propagation of the surface. The Eikonal equation of domain Ω_X can be formed as:

$$\left| \nabla T_{(x,y)} \right| * f_{(x,y)} V_{(x,y)} = 1 \tag{14}$$

where T represents the arrival time, which indicates the distance to the start point. V represents the propagation speed in Ω_X, and f is obtained by Eq. (13). The illustration of the FMM is presented in Fig. 3, where the green area represents domain Ω_X, d_x and d_y are the horizontal and vertical increments, respectively, and the orange and blue points are the neighbor points. Theirs T_x and T_y are represented as:

$$\begin{cases} T_x = \min(T_{(x+dx,y)}, T_{(x-dx,y)}) \\ T_y = \min(T_{(x,y+dy)}, T_{(x,y-dy)}) \end{cases} \tag{15}$$

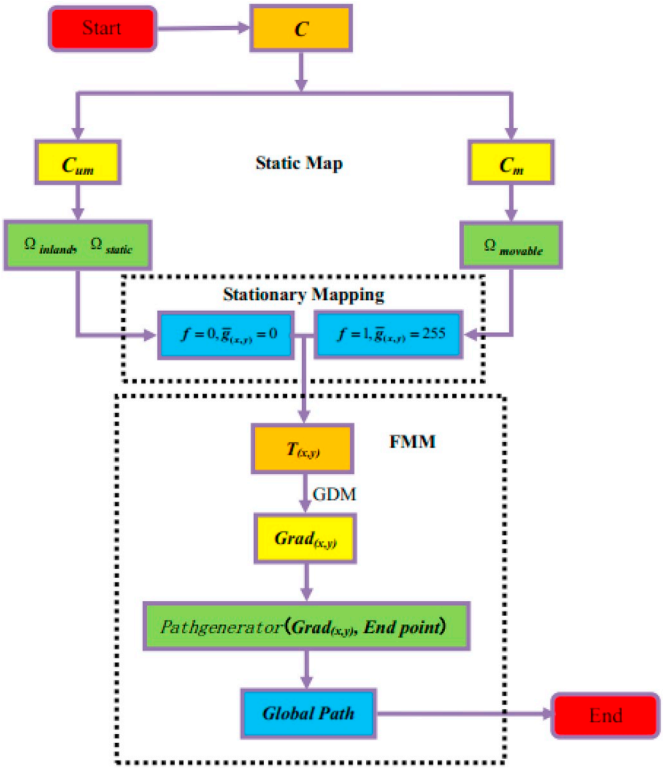

Fig. 4. Algorithm Flowchart of Global layer.

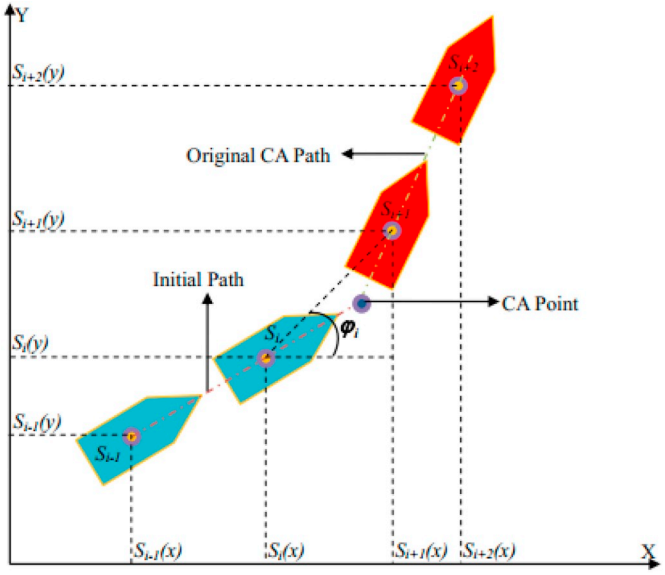

Fig. 5. Illustration of the initial CA action.

The solutions to Eq. (14) can be written as:

$$\begin{cases} T_{(x,y)} = T_x + \dfrac{1}{fV_{(x,y)}}; T_y = \inf \\ T_{(x,y)} = T_y + \dfrac{1}{fV_{(x,y)}}; T_x = \inf \\ \left(\dfrac{T_{(x,y)} - T_x}{d_x}\right)^2 + \left(\dfrac{T_{(x,y)} - T_y}{d_y}\right)^2 = (fV_{(x,y)})^{-2} \end{cases} \tag{16}$$

Based on above T obtained under $C_{m \cup um}$, we can generate the global path by applying the gradient descent method (GDM). This method can compute the gradient of T and generate the optimal global path between goal point and start point by following the direction of gradient. The flowchart of the global layer is shown in Fig. 4.

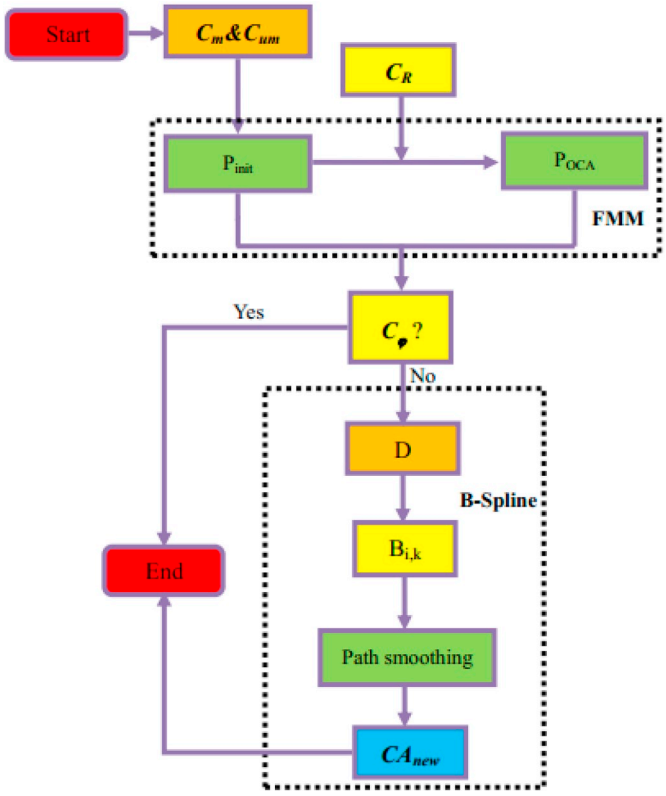

Fig. 6. Algorithm Flowchart of the collision avoidance layer.

Remark 1. During the process of grayscale processing, we first use the weighted average method to initialize the grayscale of the map, and then optimize the global segmentation result by k-means clustering.

3.2. Collision avoidance layer

3.2.1. Original collision avoidance

In order to avoid collision under constraints C_R, FMM is re-used when dynamic obstacle appears near the safety area with:

$$f\left(\Omega_{dynamic}(T_d)\right) = 1 \tag{17}$$

so that the USV can obtain the original collision avoidance (CA) path P_{OCA} while moving on the initial path P_{init}, thereby preventing the dynamic obstacle from entering the safety area. The original CA action is shown in Fig. 5, where the blue and red USVs are the positions of before and after CA, CA point is the moment when the USV begins to avoid collision, and the yaw φ_i can be determined by:

$$\varphi_i = \arctan\left(\left|\frac{S_{i+1}(y) - S_i(y)}{S_{i+1}(x) - S_i(x)}\right|\right) \tag{18}$$

3.2.2. Path smoothing

Based on the original CA in Fig. 5, the yaw-cost E_{CA} gets evaluated as follows:

$$E_{CA} = \varepsilon \max(0; \Delta\varphi_i - \phi) \tag{19}$$

where ε is the cost parameter and ϕ is the critical of consuming the energy.

The B-Spline curve of the new CA is defined by:

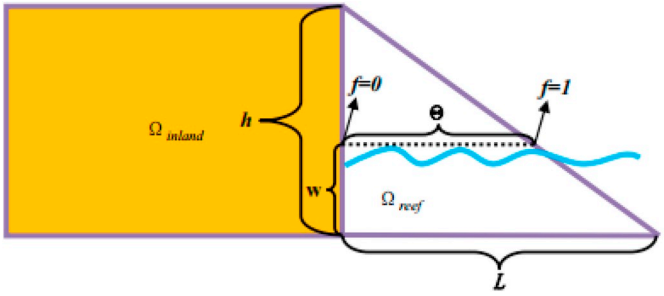

Fig. 7. Illustration of stochastic dynamic coastal environment.

$$CA_{new}(\eta) = \sum_{i}^{n} D_i B_{i,k}(\eta, \tau) \tag{20}$$

where $\eta \in (0,1)$, and the D are the control points on the P_{init} or P_{OCA}:

$$D = \left\{ \underbrace{D_1, \cdots, D_m}_{P_{init}}, \underbrace{D_{m+1}, \cdots, D_n}_{P_{OCA}} \right\} \tag{21}$$

B is the normalized B-Spline basic function, as follows:

$$\begin{cases} B_{i,0}(\eta, \tau) = \begin{cases} 0, \eta < \tau_i \vee \eta \geq \tau_{i+1} \\ 1, \tau_i \leq \eta < \tau_{i+1} \end{cases} \\ B_{i,k}(\eta, \tau) = \dfrac{\eta - \tau_i}{\tau_{i+k} - \tau_i} B_{i,k-1}(\eta, \tau) + \dfrac{\tau_{i+k+1} - \eta}{\tau_{i+k+1} - \tau_i} B_{i+1,k-1}(\eta, \tau) \\ Define: \dfrac{0}{0} = 0 \end{cases} \tag{22}$$

where k is the path smoothness factor, and τ is a non-decreasing sequence of parameters $\{0 \leq \tau_0 \leq \tau_1 \leq \cdots \leq \tau_{n+k} \leq 1\}$.

The flowchart of *CA* layer is shown in Fig. 6:

Remark 2. In comparison with the time-cost and length-cost of the USV, the yaw-cost is related to the USV motion characteristics. Extreme maneuvers in yaw would make the planned path infeasible for a USV with limited control torque, and even render the USV suffer from severe risk of capsizing. Once the initial collision avoidance path does not satisfy the constraint C_φ, the B-spline method is activated to smooth the original path, and thereby rejecting the initial collision avoidance path.

Remark 3. The nondecreasing sequence of parameters τ of the B-spline method is the node vector which decides the k-order piecewise polynomial. In Eq. (22), in order to rigorously formulate the i^{th} k-order base function $B_{i,k}(\eta, \tau)$, we require k+1 nodes $\tau_i, \tau_i + 1, \ldots, \tau_i + k$, while other nodes are invalid.

3.3. Routine correction layer

3.3.1. Stochastic dynamic coastal environments

In the SCDE, w will change around the average water level $\overline{w}_l$, as follows:

$$w \in [\overline{w}_l - \sigma, \overline{w}_l + \sigma] \tag{23}$$

where l is coastal environments parameter called hazard level that obtained by human experience, σ denotes the bound of the water level w.

In order to correct route under constraints C_r, the Poisson distribution is used to evaluate the water level w. Hence, the probability of water level w is:

$$P(w) = \frac{\overline{w}_l}{w!} e^{-\overline{w}_l} \tag{24}$$

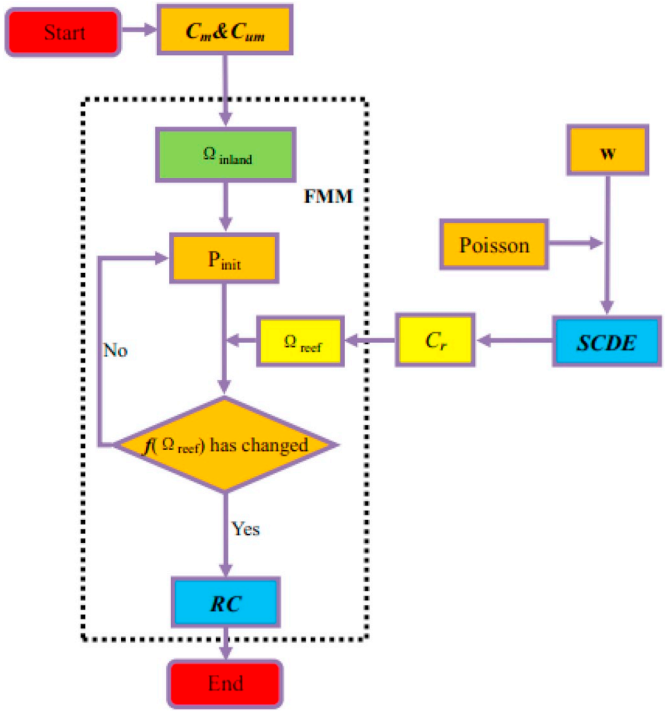

Fig. 8. Algorithm flowchart of the route correction.

The *SCDE* model in C_r can be designed by:

$$SCDE(w) = \{\Theta | \Omega_{reef}, P(w)\} \tag{25}$$

3.3.2. Routine correction

Based on the SCDE model in Eq. (25), we design the Ω_{reef} as triangle and then use Fig. 7 to illustrate the cross section of the SCDE model, where L and h are the length and height of the reefs and Θ is expressed in length. Θ can be expressed as:

$$\Theta = \frac{L}{h}(h - w) \tag{26}$$

We define $f(\Omega_{reef})$ in Θ, as follows:

$$f(\Omega_{reef}) = \frac{\gamma}{\Theta}, 0 \leq \gamma \leq \Theta \tag{27}$$

where γ is the distance from the nearest Ω_{inland}. Combined with Eqs. (13) and (16), the USV can perform *RC* while moving in the SCDE with w changing.

We design the flowchart of the route correction (RC) layer that can be shown in Fig. 8.

Remark 4. The parameter σ is defined as the bound of the water level w, since the influence range of the reefs varies with the water level. In this context, the parameter σ directly affects the scope of navigation of the USV along the coastline. In this paper, we set the σ as the value of the l.

Remark 5. If the cross section of the reef is irregular, it essentially relates to the robust separation between feasible and infeasible areas for path planning. As a preliminary idea, we may deploy or design a classifier to determine a virtual coastline rather than using the irregular one.

4. Simulation studies

In this section, the effectiveness and superiority of the MPP including backbone, CA and RC layers will be demonstrated in static or time-varying environments that divided by using K-Means clustering

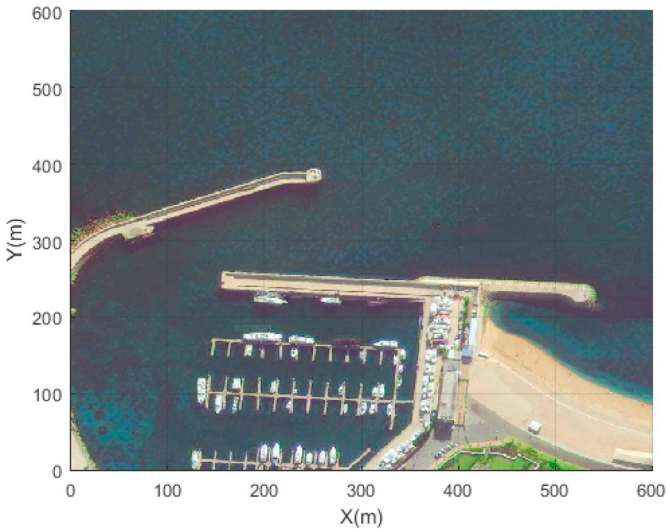

Fig. 9. Static marine environments.

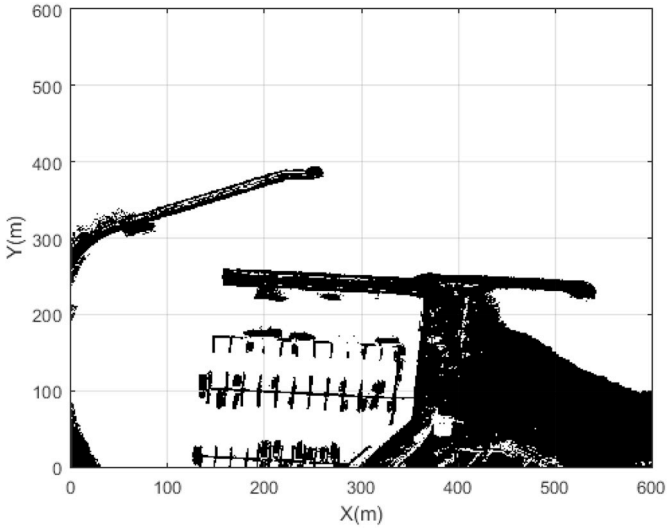

Fig. 10. K-Means electronic map.

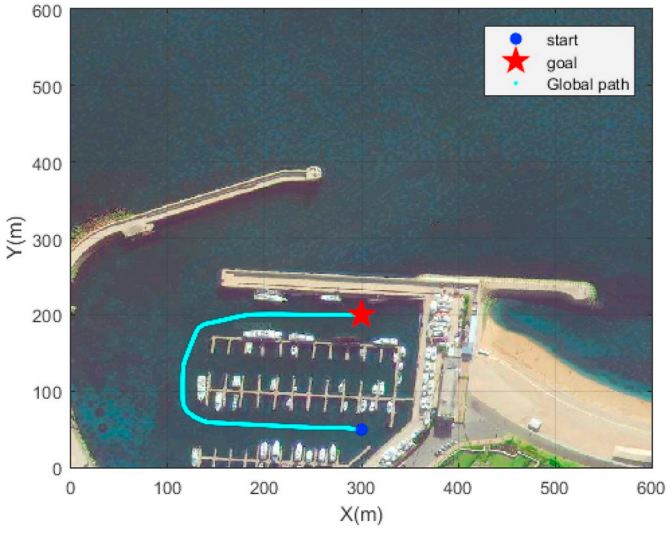

Fig. 11. Global path.

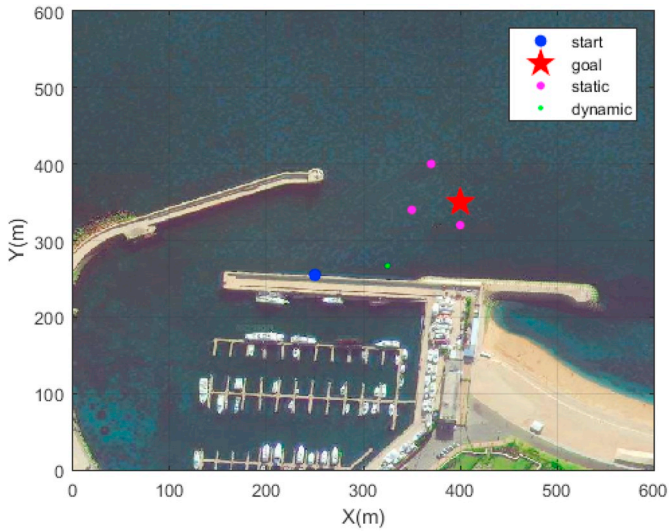

Fig. 12. Collision avoidance environments.

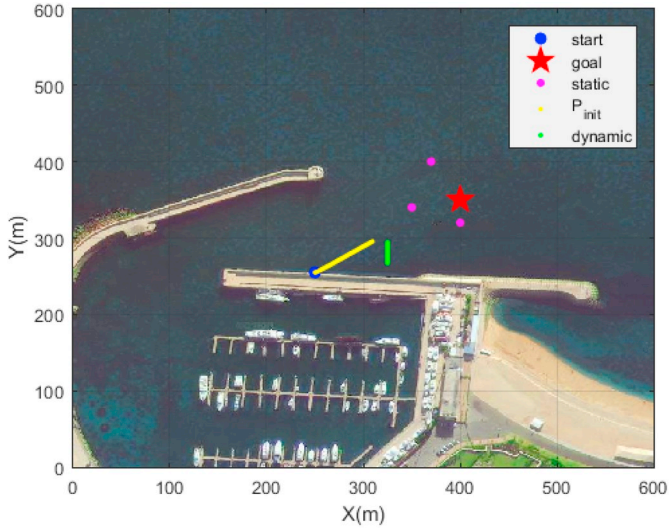

Fig. 13. Time-varying environments.

method, whereby the principal parameters are set as follows: weight $\omega_1 = \omega_2 = \omega_3 = \frac{1}{3}$, the low cluster center $\mu_1 = 0$, and the high cluster center $\mu_2 = 255$. Simulation studies are presented in the following three parts, i.e., the USV GPP using FMM, B-Spline-based path-smoothing validation and Poisson distribution-based SCDE model implementation. The MPP scheme have been coded in MATLAB R2017b version with an Intel(R) Core(TM) i7-6700 3.40 GHz CPU.

4.1. Global path planning for USV

In order to construct the static environments, the static marine environments map M_o of Dalian sea area with 600 × 600 pixels from the satellite is mainly used in the backbone layer, as shown in Fig. 9, from which we can see that this global environments mainly includes static yachts and inlands, etc., in $\Omega_{unmovable}$, and sea surface in $\Omega_{movable}$.

Based on the weight w and μ, the simulation results by K-Means clustering method are shown in Fig. 10, whereby the static marine environments are distinguished by black and white, which are unmovable and movable parts.

Since the unit size of Ω is 1, d_x and d_y are set to 1, whereby the global path with FMM is shown in Fig. 11, from which we can see that GPP with

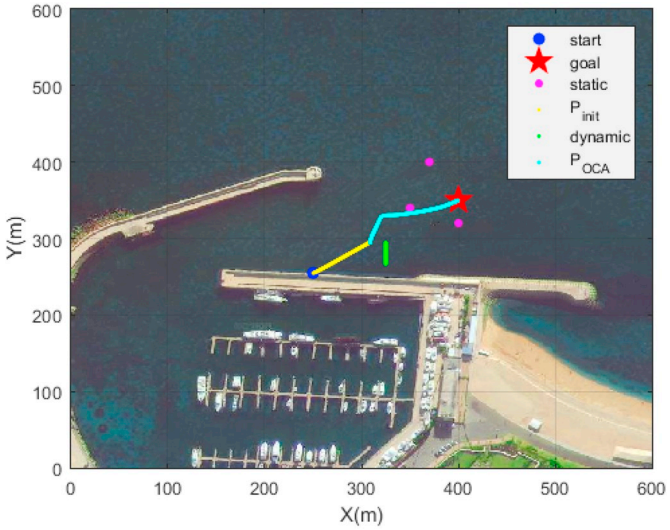

Fig. 14. Original collision avoidance.

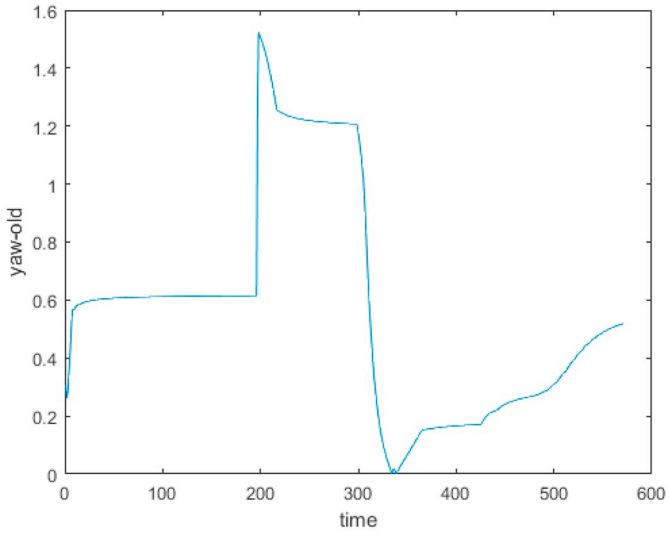

Fig. 15. The yaw φ_i pertaining to the FMM-based CA.

FMM can make the USV avoid the static obstacles and reach the goal successfully.

4.2. Collision avoidance based on B-Spline

In order to validate the smooth capability of the developed novel CA, we make domain $\Omega_{dynamic}$ in Fig. 12, from we can see that there are three static blue obstacles and a green dynamic obstacle. Note that, while the USV is moving, the dynamic obstacle is moving along the Y-axis. The time-varying environments is shown in Fig. 13.

In addition, due to the static and dynamic obstacles are added in this domain, we also use K-Means clustering method to distinguish the position of the static obstacles and the dynamic obstacles. The design parameters are chosen as follows: $R = 16$, $E_{max} = 8$, $\eta = 0.05$ and $\phi = 0.04$, the FMM-based original CA is illustrated by Fig. 14, whereby the initial yaw φ_i are shown in Fig. 15 by Eq. (18).

As can be seen from the above figure, at CA point where occur to avoid collision, φ_i has a sudden step from 0.6150 to 1.5143 that E_{CA} does not satisfy the constraint C_φ. For smoothing this path, we set three control points on P_{init} and four control points on P_{OCA}, and then use the B-Spline to generate the new CA path P_{NCA}. Here, P_{OCA} and P_{NCA} are

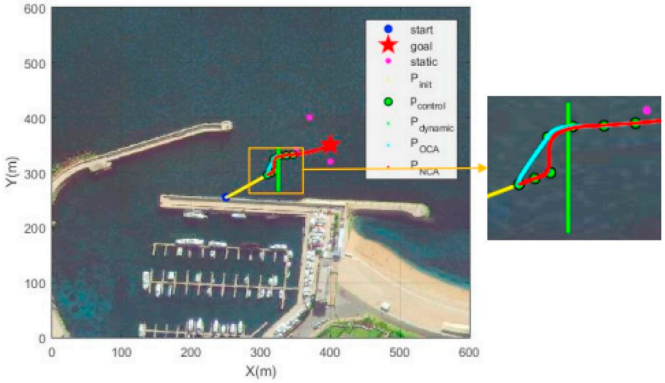

Fig. 16. Initial and smooth collision avoidance.

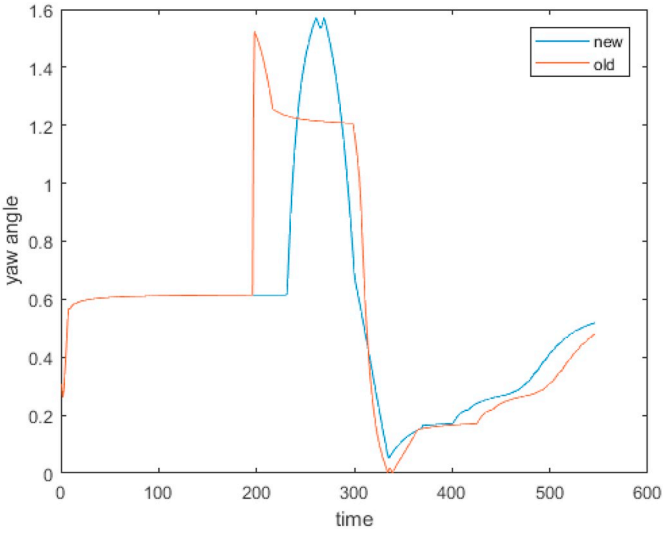

Fig. 17. Comparisons of φ_i.

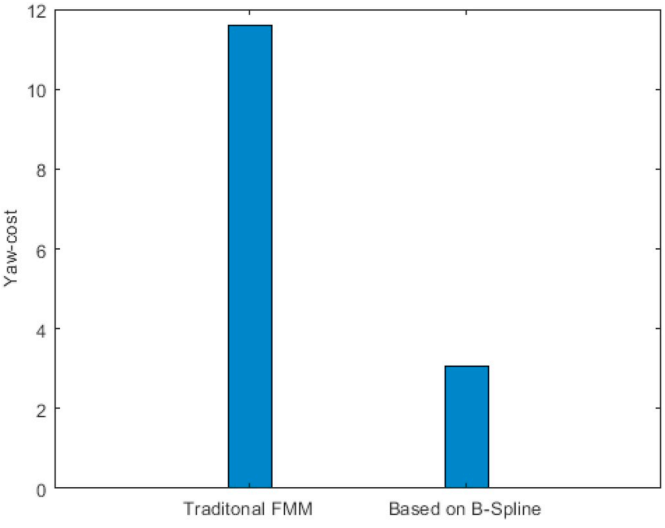

Fig. 18. Comparisons of $\sum E_{CA}$.

shown in Fig. 16, whereby the comparison results of the φ_i and $\sum E_{CA}$ with the old and new methods are shown in Figs. 17–18, from which we can see that the new method allows the USV to move a distance on P_{init} and gradually towards to P_{OCA}, instead of directly making a turning

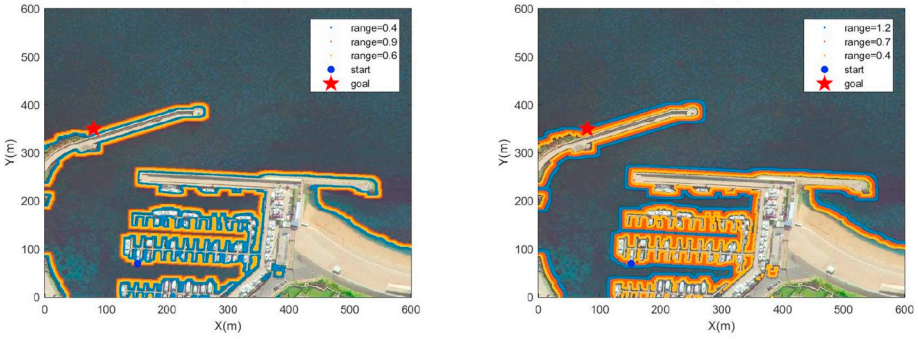

(a) $l_1 = 5$ (b) $l_2 = 10$

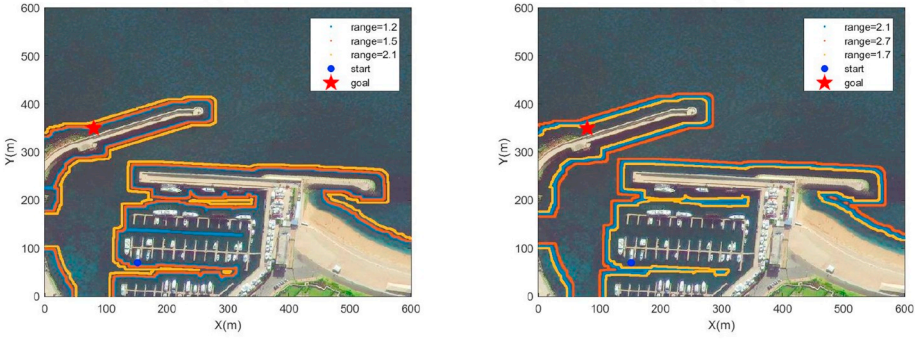

(c) $l_3 = 15$ (d) $l_4 = 20$

Fig. 19. Influence ranges comparisons.

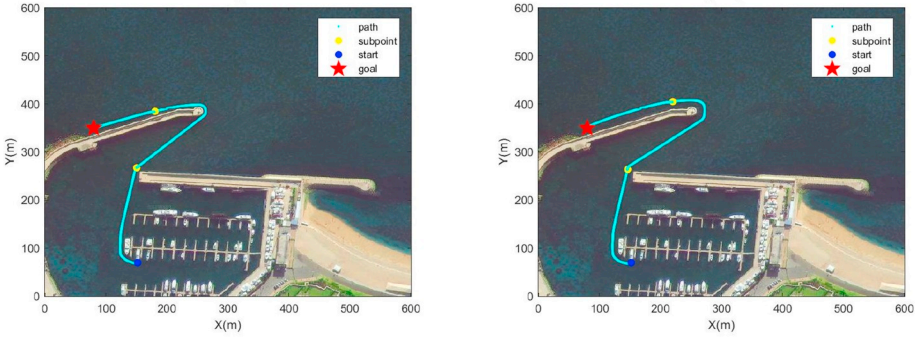

(a) $l = 5$ (b) $l = 10$

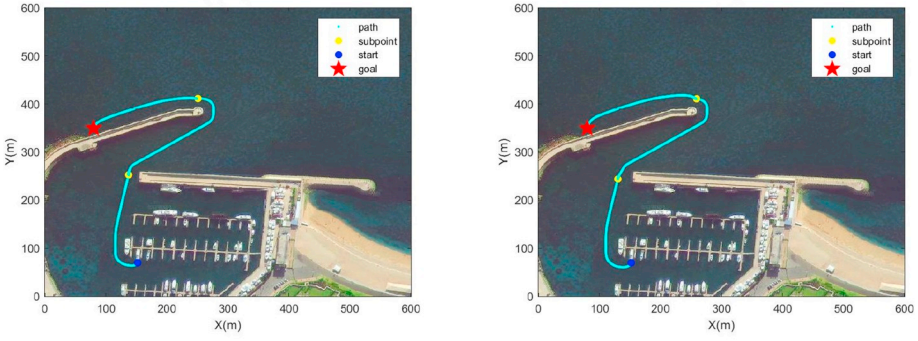

(c) $l = 15$ (d) $l = 20$

Fig. 20. Routine correction comparisons.

action at the CA point. In other word, P_{NCA} is not only safer but also smoother.

4.3. Route correction using SCDE

In order to compare the influence ranges Θ of the hazard level l in SCDE, l are chosen to equal to 5, 10, 15, 20, and the parameters of Ω_{reef} are chosen as follows: $h = 10$ and $L = 20$, which are based on environmental factors and human experience in Dalian sea area.

The simulation results which display Θ in SCDE are shown in Fig. 19, from which we can see that there are twice changes of w for each l, the higher the l, the less the $\overline{w}_l$, and the higher the w, the less the Θ. During USV moving in Ω_{reef}, each change of w leads the USV to correct route so that it can move safely. Fig. 20 shows the RC for each l.

5. Conclusion

In this paper, a multilayer path-planning (MPP) scheme has been proposed. The essence of the MPP scheme is able to collaboratively address GPP, CA and RC in the complex marine environment for the USV, within a uniformly integrated framework. The marine environments have been characterized by K-Means clustering method such that global path can be feasibly generated with the aid of the FMM in the backbone layer. By employing the B-Spline method, a new CA algorithm has been developed to smooth the original collision avoidance P_{OCA} with a lower yaw-cost in the CA layer. Using Poisson distribution, a stochastic dynamic coastal environments (SDCE) model has been derived to generate a series of real-time RC such that the planned path is safe enough around the reefs in the RC layer. Simulation results and comparisons have demonstrated that the entire MPP scheme has remarkable path-planning performance suffering from complex constraints of marine environments.

Funding

This work is supported by the National Natural Science Foundation of P. R. China (under Grants 51009017 and 51379002), the Fund for Dalian Distinguished Young Scholars (under Grant 2016RJ10), the Stable Supporting Fund of Science and Technology on Underwater Vehicle Laboratory (SXJQR2018WDKT03), and the Fundamental Research Funds for the Central Universities (under Grants 3132016314 and 3132018126).

Acknowledgment

The authors would like to thank the Editor-in-Chief, the Associate Editor, and the anonymous referees for their invaluable comments and suggestions.

References

Ammar, A., Bennaceur, H., chaari, I., Koubaa, A., Alajlan, M., 2016. Relaxed Dijkstra and A* with linear complexity for robot path planning problems in large scale grid environments. Soft computing 20 (10), 4149–4171.

Chen, X., Kong, Y., Fang, X., Wu, Q., 2013. A fast two-stage ACO algorithm for robotic path planning 2013. Neural Comput. Appl. 22 (2), 313–319.

Ferguson, D., Stentz, A., 2006. Using interpolation to improve path planning: the field D* algorithm. J. Field Robot. 23 (2), 79–101.

Garrido, S., Moreno, L., Abderrahim, M., Martin, F., 2006. Path planning for mobile robot navigation using voronoi diagram and fast marching. IEEE/RSJ International Conference on Intelligent Robots and Systems 2 (1), 2376–2381.

Hart, P.E., Nilsson, N.J., Raphael, B., 1972. A formal basis for the heuristic determination of minimum cost paths. IEEE Trans. Syst. Sci. Cybern. 4 (2), 28–29.

Kanakakis, V., Tsourveloudis, N., 2007. Evolutionary path planning and navigation of autonomous underwater vehicles. Conference on Control and Automation 1–6.

Khatib, O., 1986. Real-time obstacle avoidance for manipulators and mobile robots. Int. J. Robot. Res. 5 (1), 90–98.

Kim, Y.H., Son, W.S., Park, J.B., Yoon, T.S., 2016. Smooth path planning by fusion of artificial potential field method and collision cone approach. International conference on Measurement Instrumentation and Electronics 75, 1–4.

Kim, H., Kim, S.H., Jeon, M., Kim, J.H., Song, S., Paik, K.J., 2017. A study on path optimization method of an unmanned surface vehicle under environmental loads using genetic algorithm. Ocean. Eng. 142, 616–624.

Leigh, R., Louis, S.J., Miles, C., 2007. Using a genetic algorithm to explore A*-like pathfinding algorithms. In: IEEE Symposium on Computational Intelligence and Games, pp. 72–79.

Li, S., Sun, X., Xu, Y., 2006. Particle swarm optimization for route planning of unmanned aerial vehicles. In: International Conference on Information Acquisition, pp. 1213–1218.

Li, G., Tong, S., Cong, F., Yamashita, A., Asama, H., 2016. Improved artificial potential field-based simultaneous forward search method for robot path planning in complex environment. In: IEEE/SICE International Symposium on System Integration, pp. 760–765.

Li, Y., Ma, T., Chen, P., Jiang, Y., Wang, R., Zhang, Q., 2017. Autonomous underwater vehicle optimal path planning method for seabed terrain matching navigation. Ocean. Eng. 133, 107–115.

Li, Y., Ma, T., Wang, R., Chen, P., Zhang, Q., 2017. Terrain correlation correction method for AUV seabed terrain mapping. J. Navig. 70, 1062–1078.

Liu, Y., Bucknall, R., 2015. Path planning algorithm for unmanned surface vehicle formations in a practical maritime environment. Ocean. Eng. 97 (15), 126–144.

Liu, Y., Bucknall, R., 2017. Efficient multi-task allocation and path planning for unmanned surface vehicle in support of ocean operations. Neurocomputing 275, 1550–1566.

Liu, W., Li, Z., Li, L., Wang, F.Y., 2017. Parking like a human A direct trajectory planning solution. IEEE Trans. Intell. Transp. Syst. 18 (12), 3388–3397.

Min, H., Lin, Y., Wang, S., Wu, F., Shen, X., 2015. Path Planning of mobile robot by mixing experience with modified artificial potential field method. Mech. Eng. 7 (12), 1–17.

Pan, Z., Li, J.Q., Hu, K.M., Zhu, H., 2014. Intelligent vehicle path planning based on improved artificial potential field method. Appl. Mech. Mater. 742 (1), 349–354.

Park, C., Park, J.S., Manocha, D., 2018. Fast and bounded probabilistic collision detection for high-d of trajectory planning in dynamic environments. IEEE Trans. Autom. Sci. Eng. 15 (3), 980–991.

Pawlus, W., Karimi, H.R., Robbersmyr, K.G., 2013. Data-based modelling of vehicle collisions by nonlinear autoregressive model and feedforward neural network. Inf. Sci. 235 (6), 65–79.

Phanthong, T., Maki, T., Ura, T., Sakamaki, T., Aiyarak, P., 2014. Application of A* algorithm for real-time path re-planning of an unmanned surface vehicle avoidance underwater obstacles. J. Mar. Sci. Appl. 13 (1), 105–116.

Qin H, Wu Z, Sun Y, Chen H. Disturbance-Observer-based prescribed performance fault-tolerant trajectory tracking control for ocean bottom flying node. IEEE Access, 7: 49004-49013.

Richards, A., How, J.P., 2002. Aircraft trajectory planning with collision avoidance using mixed integer linear programming. American Control Conference 3 (3), 1936–1941.

Roberge, V., Tarbouchi, M., Labonte, G., 2013. Comparison of parallel genetic algorithm and particle swarm optimization for real-time UAV path planning. IEEE Transactions on Industrial Informatics 9 (1), 132–141.

Sethian, J.A., 1996. A fast marching level set method for monotonically advancing fronts. Proc. Natl. Acad. Sci. U. S. A 93, 1591–1595.

Shin, K., Mckay, N., 1986. A dynamic programming approach to trajectory planning of robotic manipulators. IEEE Trans. Autom. Control 31 (6), 491–500.

Song, L., Liu, Y., Bucknall, R., 2017. A multi-layered fast marching method for unmanned surface vehicle path planning in a time-variant maritime environment. Ocean. Eng. 129 (1), 301–317.

Stentz, A., 1995. The focussed D* algorithm for real-time replanning. Int. Jt. Conf. Artif. Intell. 124 (4), 1652–1659.

Tanakikorn, K., Wilson, P.A., Turnock, S.R., Philips, A.B., 2014. Grid-based GA Path Planning with Improved Cost Function for an Over-actuated Hover-Capable AUV. 2014 IEEE/OES Autonomous Underwater Vehicles (Oxford, MS, USA).

Vinay, V.P., Sridharan, R., 2012. Development and analysis of heuristic algorithms for a two-stage supply chain allocation problem with a fixed transportation cost. Int. J. Serv. Oper. Manag. 12 (12), 244–268.

Wang, N., Lv, S.L., Zhang, W.D., Liu, Z.Z., 2017. Finite-time observer based accurate tracking control of a marine vehicle with complex unknowns. Ocean. Eng. 145, 406–415.

Wang, N., Xie, G., Pan, X., Su, S.F., 2018. Full-state regulation control of asymmetric underactuated surface vehicles. IEEE Trans. Ind. Electron. https://doi.org/10.1109/TIE.2018.2890500.

Wang, N., Su, S.F., Pan, X., Yu, X., Xie, G., 2018. Yaw-guided trajectory tracking control of an asymmetric underactuated surface vehicle. IEEE Transactions on Industrial Informatics. https://doi.org/10.1109/TII.2018.2877046.

Wang, Z., Wang, L.Q., Moran, B., Zukerman, M., 2018. Application of the fast marching method for path planning of long-haul optical fiber cables with shielding. IEEE Access 6, 41367–41378.

Wang, N., Su, S.F., Han, M., Chen, W.H., 2018. Back propagating constraints based trajectory tracking control of a quadrotor with constrained actuator dynamics and complex unknowns. IEEE Transactions on Systems Man Cybernetics Systems. https://doi.org/10.1109/TSMC.2018.2834515.

Wang, N., Sun, Z., Su, S.F., Wang, Y., 2018. Fuzzy uncertainty observer-based path-following control of underactuated marine vehicles with unmodeled dynamics and disturbances. International Conference on Fuzzy Theory and its Applications. https://doi.org/10.1007/s40815-018-0522-3.

Wang, N., Sun, Z., Yin, J., Zou, Z., Su, S.F., 2019. Fuzzy unknown observer-based robust adaptive path following control of underactuated surface vehicles subject to multiple unknowns. Ocean. Eng. 176, 57–64.

Wang, N., Karimi, H.R., Li, H., Su, S.F., 2019. Accurate trajectory tracking of disturbed surface vehicles: a finite-time control approach. IEEE ASME Trans. Mechatron. https://doi.org/10.1109/TMECH.2019.2906395.

Wu, P., Xie, S., Liu, H., Li, M., Li, H., Peng, Y., Li, X., Luo, J., 2016. Autonomous obstacle avoidance of an unmanned surface vehicle based on cooperative manoeuvring. Ind. Robot 44, 64–74.

Wu, Z., Hu, G., Feng, L., Wu, J., Liu, S., 2016. Collision avoidance for mobile robots based on artificial potential field and obstacle envelope modelling. Assemb. Autom. 36 (3), 318–332.

Zhou, Z., Ding, J., Huang, H., Takei, R., Tomlin, C., 2018. Efficient path planning algorithms in reach-avoid problem. Automatica 89, 28–36.